SUPPLEMENTAL FIGURES

Figure S1: Targeting of *Per2* gene with a color-switching luciferase cassette (related to Figure 1).

(**A**) Diagram of the knock-in construct targeted to the *Per2* locus. Southern blotting probes are indicated with 5'Probe and 3'Probe. 5'F and 5'R are the primer pair used in 5' long fragment PCR. 3'F and 3'R are used in 3' long fragment PCR. EcoRI and EcoRV sites indicated in the diagram are the restriction sites for Southern blotting. Neo is the neomycin resistance cassette, and DT is the diphtheria toxin cassette on the 5' arm of the construct. (**B**) Southern blotting and long-fragment PCR (**C**) to verify the gene targeting in the ES cell clones. (**D**) Homozygous and heterozygous germline transduction in mice were tested by Southern blot. (**E**) Split channels of the dual-color imaging from the VIP-Cre and AVP-Cre SCN slices shown in **Figure 1**, compared with the merged images.

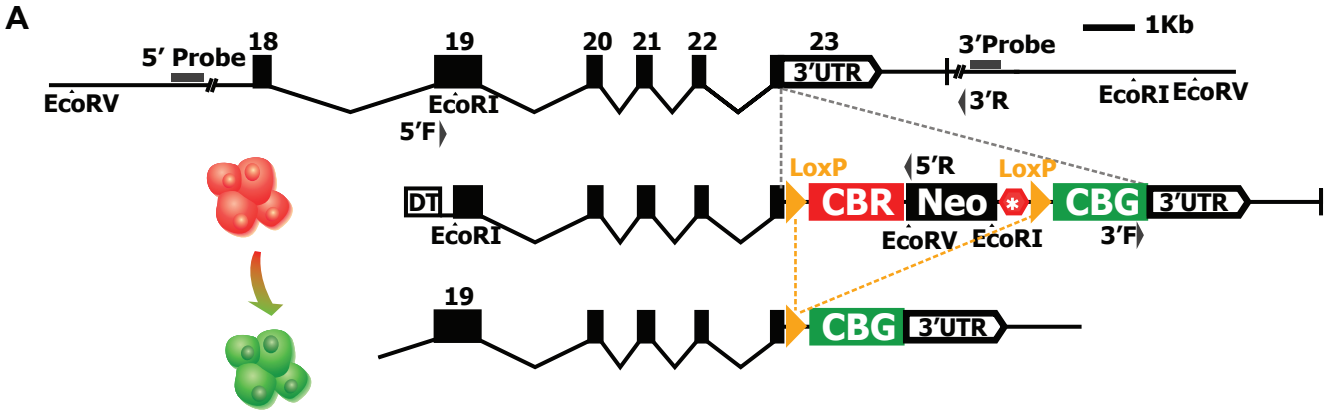
A
5′ Probe
18
19
20
21
22
23
3′UTR
3′Probe
1Kb
EcoRV
EcoRI
5′F
3′R
EcoRI
EcoRV
LoxP
5′R
LoxP
DT
CBR
Neo
CBG
3′UTR
EcoRI
EcoRV
EcoRI
3′F
19
CBG
3′UTR

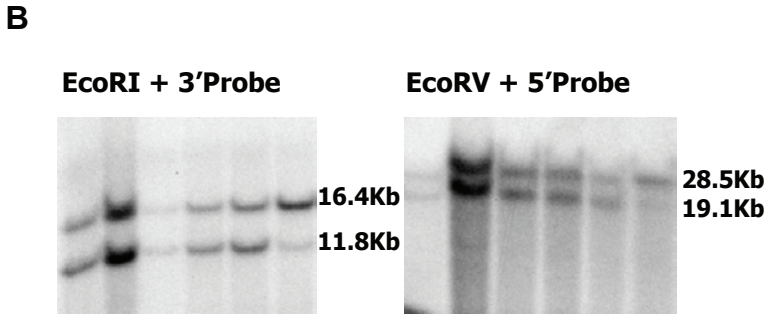
B
EcoRI + 3′Probe
EcoRV + 5′Probe
16.4Kb
11.8Kb
28.5Kb
19.1Kb

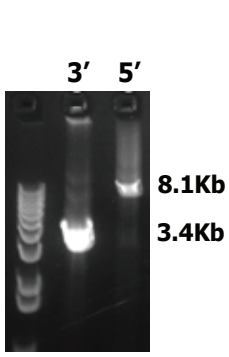
C
3′
5′
8.1Kb
3.4Kb


D
homo
hetero
wild-type

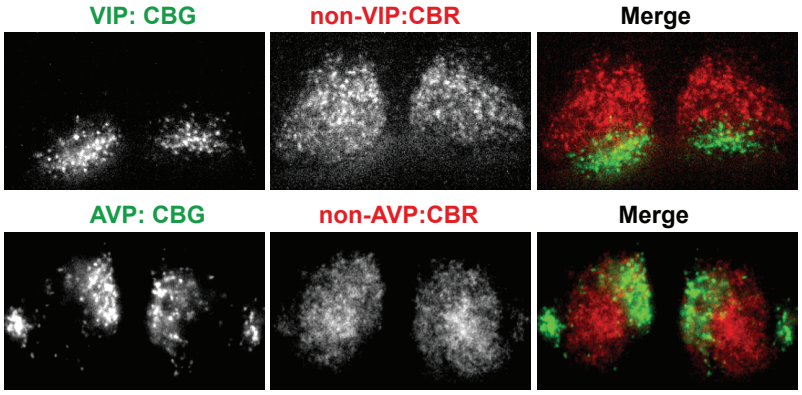
E
VIP: CBG
non-VIP:CBR
Merge
AVP: CBG
non-AVP:CBR
Merge

Figure S2. Analysis pipeline for single-cell rhythmicity (related to STAR Methods, Analysis of bioluminescence signals).

Raw signals from single-cell trajectories were filtered by removing outliers and then detrended with a Hodrick-Prescott (HP) filter. (**A**) shows the green HP baseline estimated from the black raw signal and (**B**) shows the baseline-subtracted data. Detrended data carries high-frequency low-amplitude read noise, and an eigen decomposition of the autocorrelation matrix and an eigenvector-based signal reconstruction are performed to remove the low-amplitude noise, as shown in (**C**), with X axis as the eigenvalue index and Y axis as the eigenvalue. Denoised data is reconstructed and shown as the red trajectory in (**D**). To analyze the rhythmicity of detrended and denoised signals, Lomb-Scargle spectral analysis is performed and the resulting LS periodogram is shown in (**E**), with X axis as the period range and Y axis as the normalized power value. The power peak between 18-30 hr is used to estimate of period of the signal, and a sinusoid curve-fit, with a constraint of ±1 hr of the LS peak period, is performed to estimate the rhythmicity including fitted period, phase, amplitude and damping rate. The fitted cosine trajectory is shown in blue in (**F**). (**G-L**) shows the same analysis procedure as in (**A-F**), where (**A-F**) is a typical rhythmic cell from the AVP-Cre SCN, while (**G-L**) shows a noisy cell from the AVP-*Bmal1*$^{-/-}$ SCN that does not fit to a cosine model.

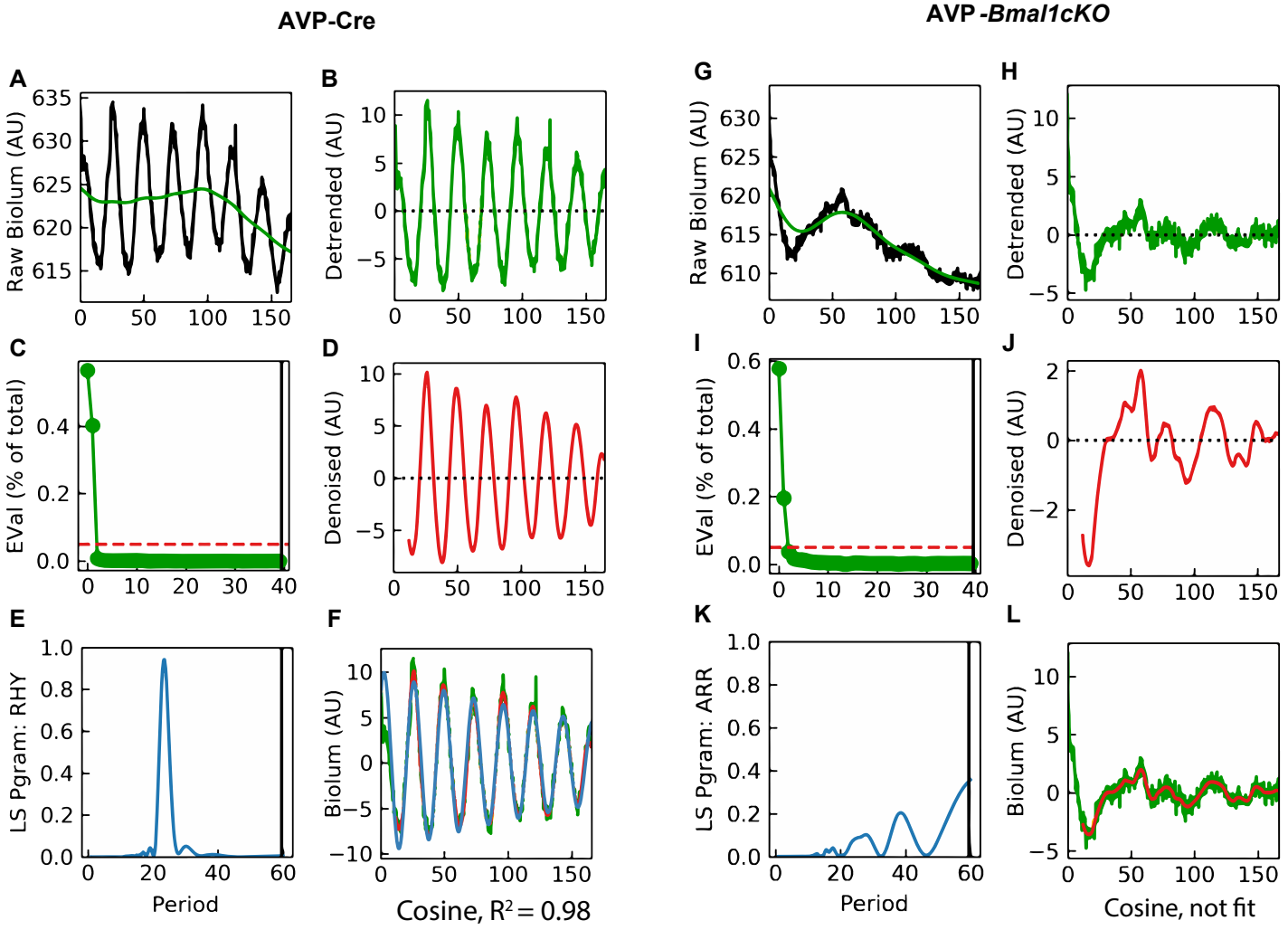
AVP-Cre
AVP -Bmal1cKO
A
B
C
D
E
F
G
H
I
J
K
L
Raw Biolum (AU)
Detrended (AU)
EVal (% of total)
Denoised (AU)
LS Pgram: RHY
Biolum (AU)
LS Pgram: ARR
Period
Cosine, R² = 0.98
Cosine, not fit

Figure S3: Single-cell quantification of Cre-only and *Bmal1*$^{-/-}$ SCN slices (related to Figures 1, 2, 3, and 4).

(**A**) Rayleigh plots of circular mean of the 4th-day phases from VIP-Cre and AVP-Cre SCN slices during pre-culture (VIP, n=5; AVP, n=6). Each replicate is represented by a point in the overlaid circular scatter plot. Mean phases of green, Cre positive cells are zeroed to red control cells for statistical analysis between cell types. (**B**) The average green signal of Cre-positive cells across the recording during pre-culture, TTX treatment or washout, was background subtracted and normalized the to average red signal of non-Cre cells in each SCN (AVP-Cre, n=5; AVP-*Bmal1*$^{-/-}$, n=4; VIP-Cre, n=3; VIP-*Bmal1*$^{-/-}$, n=4). * Significant difference ($p<0.05$) from one-way ANOVA with multiple comparisons is shown. (**C, D**) Mean +/- SEM of MIC scores are shown to compare the associations between or inside the two lobes of an SCN. The between lobe associations were categorized as green-green-inter, red-red inter and green-red inter and the within lobe associations were categorized as green-green-intra, red-red intra and green-red intra. Each mean MIC value from a replicate is represented by a point in the overlaid scatter plot (VIP-Cre, n=3; VIP-Bmal1$^{-/-}$, n=4; AVP-Cre, n=5; AVP-Bmal1$^{-/-}$, n=4). Nonsignificant differences between the inter- and intra-lobe comparison of each condition are not shown. **(E-L)** Cell trajectories were classified as rhythmic (p-value of peak <0.05) or arrhythmic (p-value of peak ≥ 0.05) with Lomb-Scargle periodogram between 18-30 hr, as described in **Supplemental Methods**. (**E-F**) Mean +/- SEM periods of VIP-Cre (n=3) and VIP-*Bmal1*$^{-/-}$ SCN slices (n=4). Green represents the VIP-cre cells and red represents non-VIP cells. Lower asterisks indicate significance of t-tests between green and red cells, and upper asterisks indicate significance of Holm-Sidak's multiple comparisons test within green cells. (**G-H**) Mean +/- SEM LSP rhythmicities of VIP-Cre and VIP-*Bmal1*$^{-/-}$ SCN slices. Lower asterisks indicate significance of t-tests between green and red cells, and upper asterisks indicate significance of Holm-Sidak's multiple comparisons test within green cells. (**I-J**) Mean +/- SEM periods of AVP-Cre and AVP-*Bmal1*$^{-/-}$ SCN slices (AVP-Cre n=5; AVP-*Bmal1*$^{-/-}$ n=4). Green represents the AVP-Cre cells and red represents non-AVP cells. (**K-L**) Mean +/- SEM LSP rhythmicities of AVP-Cre and AVP-*Bmal1*$^{-/-}$ SCN slices (* $p \leq 0.05$; ** $p \leq 0.01$; *** $p \leq 0.001$). Detailed quantification results and ANOVA analyses are included in **Supplemental Data 1**.

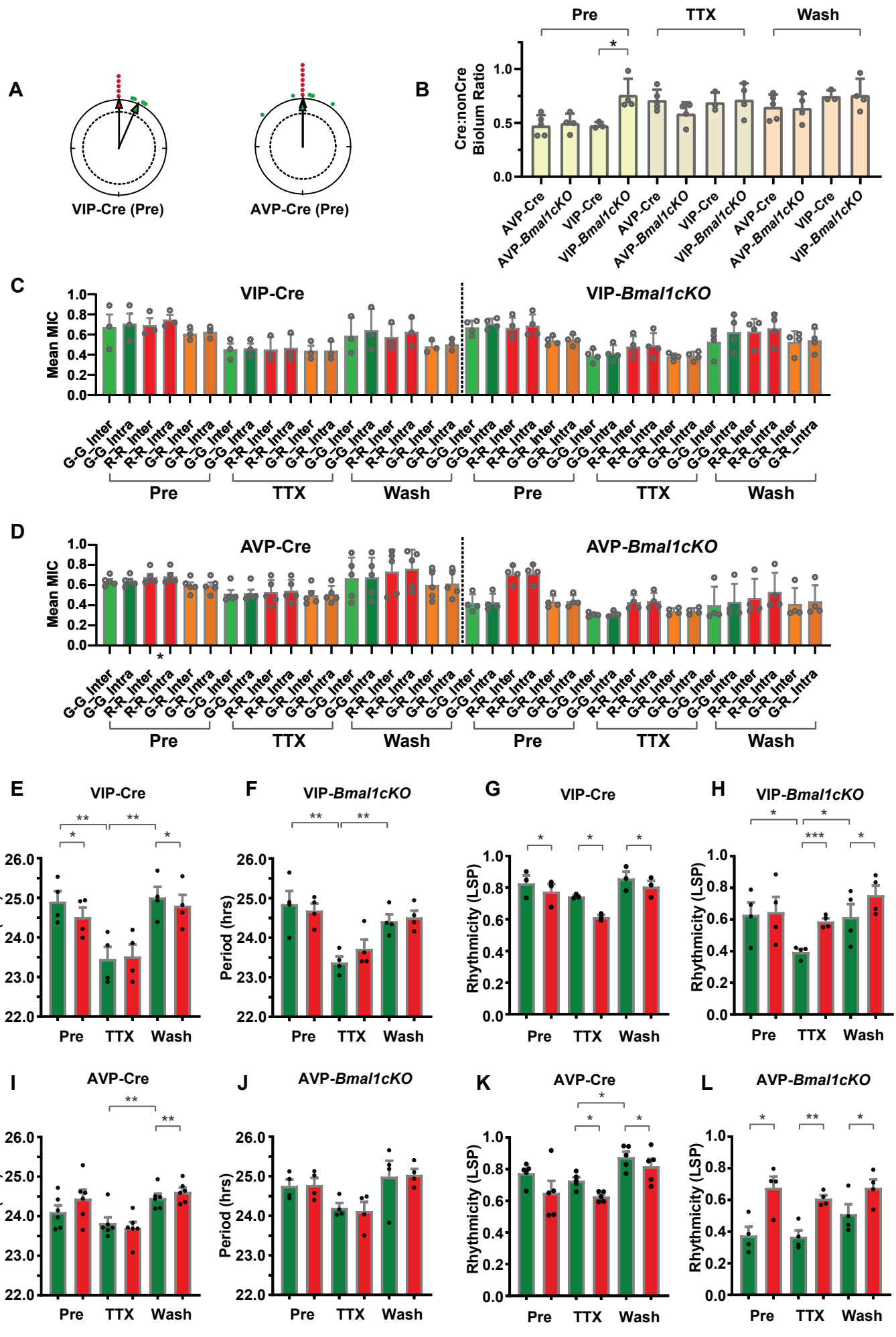
A
VIP-Cre (Pre)
AVP-Cre (Pre)
B
Pre
TTX
Wash
Cre:nonCre Biolum Ratio
AVP-Cre
AVP-Bmal1cKO
VIP-Cre
VIP-Bmal1cKO
C
VIP-Cre
VIP-Bmal1cKO
Mean MIC
G-G_Inter
G-G_Intra
R-R_Inter
R-R_Intra
G-R_Inter
G-R_Intra
Pre
TTX
Wash
D
AVP-Cre
AVP-Bmal1cKO
E
VIP-Cre
F
VIP-Bmal1cKO
G
VIP-Cre
H
VIP-Bmal1cKO
Period (hrs)
Rhythmicity (LSP)
I
AVP-Cre
J
AVP-Bmal1cKO
K
AVP-Cre
L
AVP-Bmal1cKO

Figure S4: Single-cell rhythmicity and network analysis of SCN explants with genetic excision of *Bmal1* in both VIP and AVP cells (related to Figures 2, 3, and 4).

(**A**) Single-cell trajectories from a VIP/AVP-*Bmal1*$^{-/-}$ SCN through pretreatment, TTX treatment and washout of TTX. (**B**) Heat map representations of the single-cells from the same SCN slices. (**C-D**) LSP rhythmicity values shown by anatomical location in the SCN. The histogram shows LSP Rhythmicity distributions of *Bmal1*$^{-/-}$ cells versus VIP/AVP-Cre cells. (**E**) Pairwise MIC score plot of neurons in the VIP/AVP-*Bmal1*$^{-/-}$ SCN. (**F**) Correlation network constructed from pair-wise MIC analysis. (**G**) Mean +/- SEM plots of MIC scores from the VIP/AVP-*Bmal1*$^{-/-}$ SCN slices (n=4) * p value ≤0.05; ** p value ≤ 0.01; *** p value ≤ 0.001. Detailed quantification results are included in **Supplemental Data 1**.

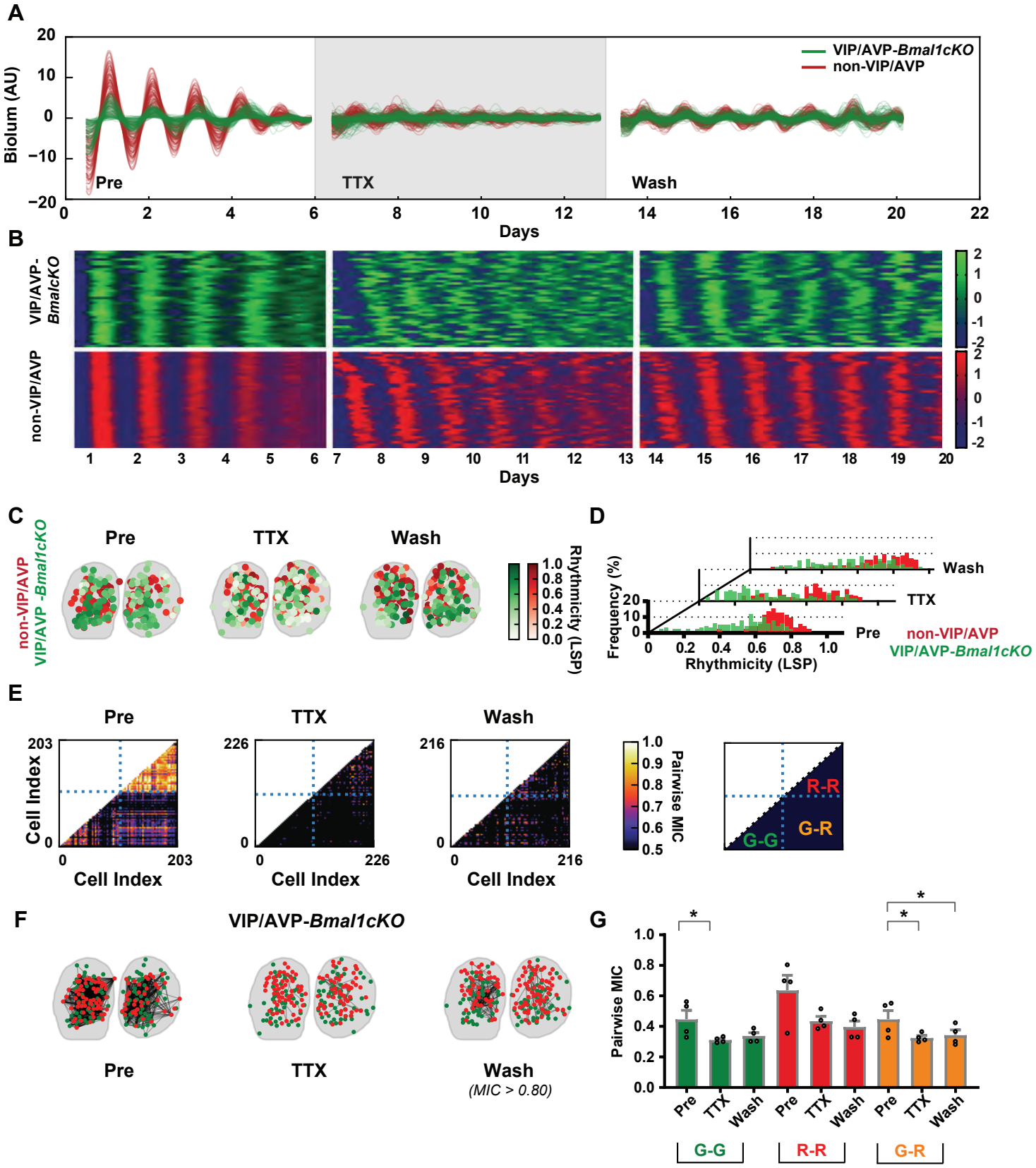
A
Biolum (AU)
VIP/AVP-Bmal1cKO
non-VIP/AVP
Pre
TTX
Wash
Days
B
VIP/AVP-BmalcKO
non-VIP/AVP
Days
C
non-VIP/AVP
VIP/AVP -Bmal1cKO
Pre
TTX
Wash
Rhythmicity (LSP)
D
Frequency (%)
Wash
TTX
Pre
non-VIP/AVP
VIP/AVP-Bmal1cKO
Rhythmicity (LSP)
E
Pre
TTX
Wash
Cell Index
Pairwise MIC
R-R
G-G
G-R
F
VIP/AVP-Bmal1cKO
Pre
TTX
Wash
(MIC > 0.80)
G
Pairwise MIC
Pre
TTX
Wash
G-G
R-R
G-R

Figure S5: Circadian activity rhythms in Cre-only Control, VIP-*Bmal1*$^{-/-}$, AVP-*Bmal1*$^{-/-}$, and VIP/AVP-*Bmal1*$^{-/-}$ mice (related to Figures 2, 3, 4, and 5).

Circadian wheel-running activity of mice with light cycle treatments as follows: LD1, animals were maintained in regular LD12:12 cycles for at least two weeks; DD1, animals were released into constant darkness for three weeks; LL, constant light for 2-3 weeks; DD2, constant darkness for three weeks; LD2, LD12:12 light dark cycle for three weeks for re-entrainment; DD3, constant darkness for three weeks. (**A - D**) Actogram of the circadian behavioral activity of a Cre-only control, a VIP-*Bmal1*$^{-/-}$, an AVP-*Bmal1*$^{-/-}$ and a VIP/AVP-*Bmal1*$^{-/-}$ mouse. (**E**) Constant darkness epochs DD1, DD2 and DD3 were used to calculate the period length of circadian rhythms. Scatter plots of the three period values are overlaid with the box plot showing median line, Turkey whiskers and the point of mean (DD2: Cre-only control, 23.73hrs, n=18; VIP-*Bmal1*$^{-/-}$, 23.66hrs, n=22; AVP-*Bmal1*$^{-/-}$, 24.05hrs, n=15; VIP/AVP-*Bmal1*$^{-/-}$, 23.91hrs, n=13). Asterisks indicate the significance of Holm-Sidak's multiple comparison between DD2, with ANOVA adjusted P value from the four DD2 groups. (**F**) Average variance in period for each animal, calculated from the six DD periods from **G** is compared among wildtype, VIP-*Bmal1*$^{-/-}$, AVP-*Bmal1*$^{-/-}$ and VIP/AVP-*Bmal1*$^{-/-}$. Detailed quantification results and are included in **Table S4.** (**G**) Period lengths calculated from two 10-day sub-intervals in each of the three constant darkness: DD1-1, DD1-2, DD2-1, DD2-2, DD3-1 and DD3-2. Each line connecting six data points are derived from the same animal. * $p \leq 0.05$; ** $p \leq 0.01$; *** $p \leq 0.001$. Detailed quantification results are included in **Supplemental Data 2**.

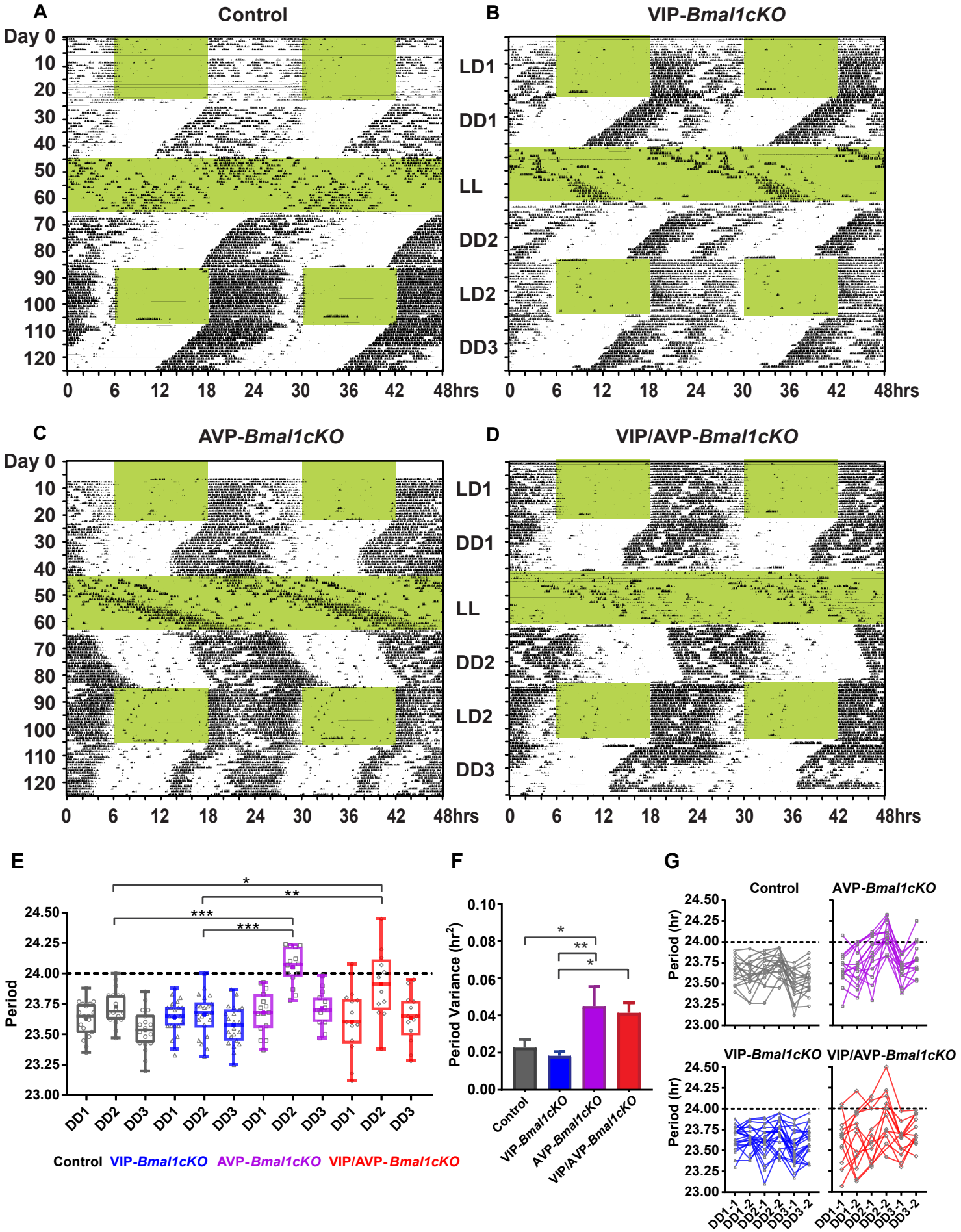
A
Control
Day 0
10
20
30
40
50
60
70
80
90
100
110
120
0
6
12
18
24
30
36
42
48hrs
B
VIP-Bmal1cKO
LD1
DD1
LL
DD2
LD2
DD3
C
AVP-Bmal1cKO
D
VIP/AVP-Bmal1cKO
E
Period
24.50
24.25
24.00
23.75
23.50
23.25
23.00
DD1
DD2
DD3
Control
VIP-Bmal1cKO
AVP-Bmal1cKO
VIP/AVP-Bmal1cKO
F
Period Variance (hr2)
0.10
0.08
0.06
0.04
0.02
0.00
G
Period (hr)
DD1-1
DD1-2
DD2-1
DD2-2
DD3-1
DD3-2

Figure S6: Testing the role of neurotransmission strength and cell types in SCN synchrony (related to Figure 6).

A mini-SCN model was created and neurotransmission strength (**A-B**) and cell type ratios (**C-D**) were tested to determine if these parameters could account for the observed experimental phenotypes. Details are included in **methods**. (**A**) Diagram of the mini-SCN model for varying coupling strength. Three cellular populations (AVP, VIP, nonAVP nonVIP) of 20 cells each were connected via mean-field coupling, with the strength of the signals from each population varied. (**B**) To test the hypothesis that difference in neurotransmission strength is sufficient to explain the observed phenotypes, we varied the relative strength of coupling between 1:10 and 10:1 AVP:VIP. Resulting whole-SCN mean MIC scores for 100 simulations each of control, VIP-*Bmal1*$^{-/-}$ (cKO), and AVP-*Bmal1*$^{-/-}$ (cKO) models are shown. We considered a model to replicate the phenotype if control and VIP-*Bmal1*$^{-/-}$ showed significantly higher ($p<0.05$) mean MIC scores than AVP-*Bmal1*$^{-/-}$, and showed no significant difference ($p>0.05$) between each other (two-sided Mann-Whitney U-test with Bonferroni correction for 21 individual tests). This was true in two cases (denoted by asterisks), 5:1 and 10:1 AVP:VIP. Thus, stronger neurotransmission are sufficient to recapitulate the observed experimental phenotypes. (**C**) Diagram of the mini-SCN model where cell counts of VIP and AVP cells were varied. Neurotransmission strength was fixed at 1:1 AVP:VIP. (**D**) To test the hypothesis that the experimental phenotype is mediated by relative fractions of AVP and VIP cells, we varied the 40 AVP:VIP cell counts from 4:36 to 36:4 AVP:VIP. As with coupling strength, the phenotype (described above) was recapitulated when AVP cells greatly outnumber VIP cells (9:1). Thus, coupling strength, as mediated by a stronger AVP neurotransmission pathway or an abundance of AVP cells, is sufficient to explain the observed experimental differences between AVP and VIP coupling, and implicates AVP as of importance in SCN synchrony. (**E**) Distributions of pairwise MIC score of the three SCN genotypes during one simulation of resynchronization. (**F**) Heat map plots of z-score and Rayleigh plots of phases of single-cell trajectories are shown in the same color modes as in A and B. Each heat map includes 20 example cells of the corresponding cell type. Phases for the Rayleigh plot were estimated at the end of the sixth day.

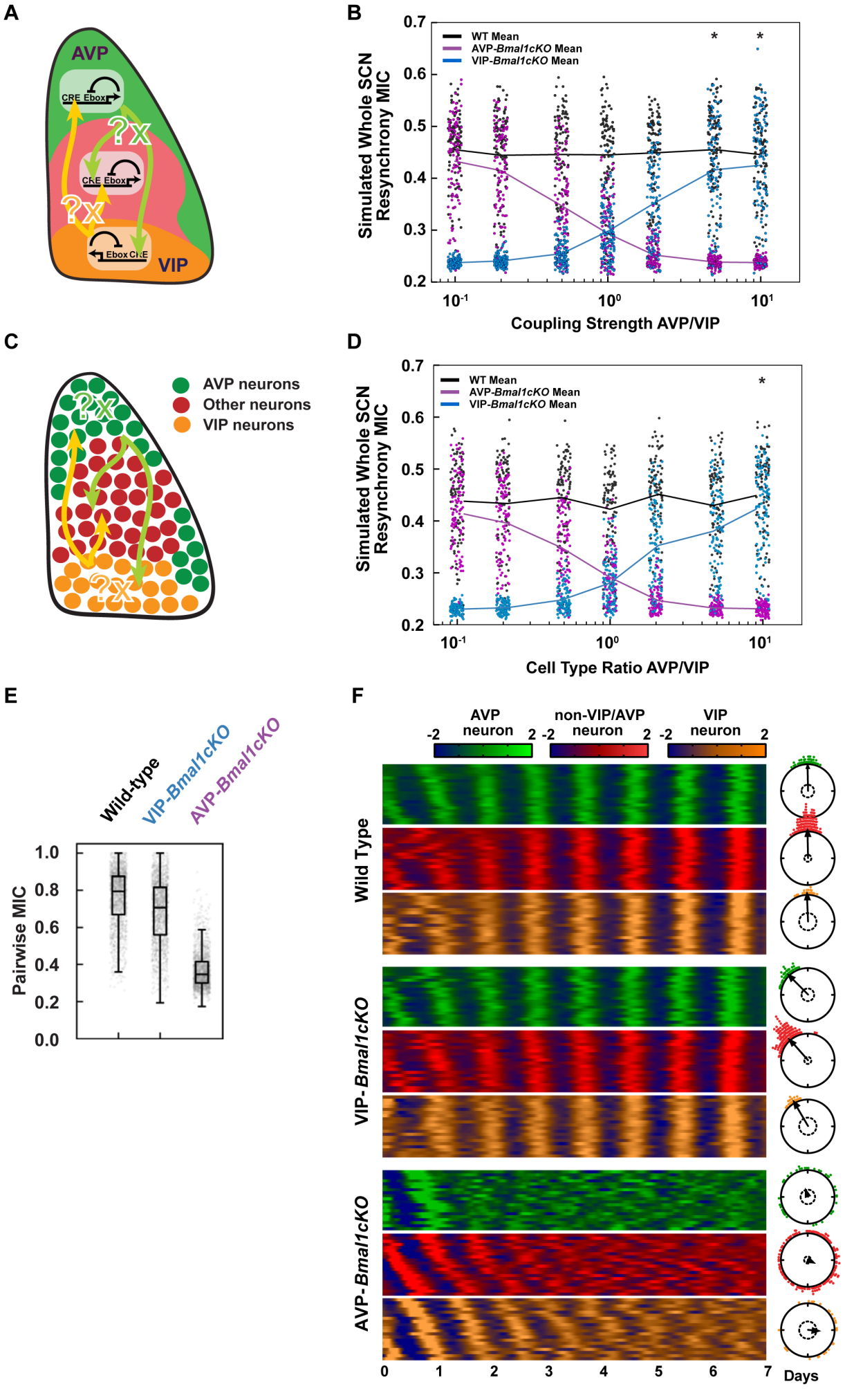
A
AVP
CRE Ebox
?x
CRE Ebox
?x
Ebox CRE
VIP
B
WT Mean
AVP-Bmal1cKO Mean
VIP-Bmal1cKO Mean
Simulated Whole SCN Resynchrony MIC
Coupling Strength AVP/VIP
C
AVP neurons
Other neurons
VIP neurons
D
Cell Type Ratio AVP/VIP
E
Wild-type
VIP-Bmal1cKO
AVP-Bmal1cKO
Pairwise MIC
F
AVP neuron
non-VIP/AVP neuron
VIP neuron
Wild Type
VIP-Bmal1cKO
AVP-Bmal1cKO
Days

SUPPLEMENTAL TABLES

Supplemental Table 1: Genotypes of mouse lines used in experiments (Related to Figures 2, 3, and 4 and STAR Methods, Mice).

Supplemental Table 1: Genotypes of mouse lines used in experiments.		
Abbreviations	**Full Description of Genotypes**	**Phenotype**
AVP-Cre	*AVP$^{iCre/+}$; Bmal1$^{+/+}$; Per2$^{iLuc/iLuc}$*	Normal Rhythms
VIP-Cre	*VIP$^{Cre/+}$; Bmal1$^{+/+}$; Per2$^{iLuc/iLuc}$*	Normal Rhythms
AVP-*Bmal1cKO or* AVP-*Bmal1$^{-/-}$*	*AVP$^{iCre/+}$; Bmal1$^{fx/fx}$; Per2$^{iLuc/iLuc}$*	Lengthened periods and increased period variances
VIP-*Bmal1cKO or VIP-Bmal1$^{-/-}$*	*VIP$^{Cre/+}$; Bmal1$^{fx/fx}$; Per2$^{iLuc/iLuc}$*	Normal Rhythms
VIP/AVP-*Bmal1cKO or VIP/AVP-Bmal1$^{-/-}$*	*AVP$^{iCre/+}$; VIP-Cre; Bmal1$^{fx/fx}$; Per2$^{iLuc/iLuc}$*	Lengthened periods and increased period variances
NMS-Cre	*NMS$^{iCre/+}$; Bmal1$^{+/+}$; Per2$^{iLuc/iLuc}$*	Normal Rhythms
NMS-*Bmal1cKO*	*NMS$^{iCre/+}$; Bmal1$^{fx/fx}$; Per2$^{iLuc/iLuc}$*	Desynchronized
Control (**Figure 5**)	*AVP$^{iCre/+}$; Per2$^{iLuc/iLuc}$* *VIP$^{iCre/+}$; Per2$^{iLuc/iLuc}$* *Per2$^{iLuc/iLuc}$*	Normal Expression

Supplemental Table 2: Rhythmicity and synchrony of *Bmal1*$^{-/-}$ SCN during the decoupling and recoupling processes (Related to Figures 2, 3, 4, and 5). Results of *Bmal1*$^{-/-}$ SCNs are presented in comparison to wildtype controls (one-way ANOVA of mean from multiple slices). VIP/AVP-*Bmal1*$^{-/-}$ is compared to AVP-Cre controls. The synchrony of red cells is not affected during pretreatment, which is likely to represent an *in vivo* entrainment by light-dark cycles. MIC quantification during TTX treatment is excluded because the circuit and coupling was turned off with TTX. * Synchrony between red cells with normal *Bmal1*, in the AVP-*Bmal1*$^{-/-}$ or VIP/AVP-*Bmal1*$^{-/-}$ SCN, are not affected during pretreatment, which is likely to represent an *in vivo* entrainment by light-dark cycles. $^{\#}$ Some *Bmal1*$^{-/-}$ cells in the ventral part of VIP/AVP-*Bmal1*$^{-/-}$ SCN are not affected during pretreatment, which are possibly the VIP cells driven by the entrained network during pretreatment.

Genotypes	Treatments	Coupling (MIC)		
		VIP : VIP (G-G)	VIP : nonVIP (G-R)	nonVIP : nonVIP (R-R)
VIP- *Bmal1cKO*	Pre	Unaffected	Unaffected	Unaffected
	TTX	N/A	N/A	N/A
	Wash	Unaffected	Unaffected	Unaffected
Genotypes	Treatments	Coupling (MIC)		
		AVP : AVP (G-G)	AVP : nonAVP (G-R)	nonAVP : nonAVP (R-R)
AVP- *Bmal1cKO*	Pre	↓	↓	Unaffected*
	TTX	N/A	N/A	N/A
	Wash	↓	↓	↓
Genotypes	Treatments	Coupling (MIC)		
		VA : VA (G-G)	VA: nonVA (G-R)	nonVA : nonVA (R-R)
VIP/AVP- *BmalcKO*	Pre	↓$^{\#}$	↓$^{\#}$	Unaffected*
	TTX	N/A	N/A	N/A
	Wash	↓	↓	↓